Intracrystalline Structure and Physicochemical Properties of Mixed SiO_2−TiO_2 Sol-Pillared Aluminosilicate

Joo-Hyoung Park,[†] Jae-Hun Yang,[†,‡] Joo-Byoung Yoon,[†] Seong-Ju Hwang,[‡] and Jin-Ho Choy*[,‡]

School of Chemistry and Molecular Engineering, Seoul National University, Seoul 151-747, Korea, and Center for Intelligent Nano-Bio Materials (CINBM), Division of Nano Sciences and Department of Chemistry, Ewha Womans Univeristy, Seoul 120-750, Korea

Received: October 1, 2005; In Final Form: November 28, 2005

Highly porous layered inorganic−inorganic nanohybrids were prepared by pillaring SiO_2−TiO_2 nanosol particles with aluminosilicate layers. According to powder X-ray diffraction analysis, the basal spacing of SiO_2−TiO_2 pillared aluminosilicate (STPC) calcined at 400 °C was determined to be larger than 40 Å. N_2 adsorption−desorption isotherm measurements showed the STPC to have a large Brunauer−Emmett−Teller surface area of ∼590 m^2/g, of which approximately 70% originates from micropores with a size range of 8−16 Å. The sorption behavior of various solvent vapors such as hexane, methanol, and water reveals internal pore surfaces of the STPC to be hydrophobic. A distinct blue shift of absorption edge in UV−vis spectra clearly demonstrates that the nanosized TiO_2 particles are formed between silicate layers as a pillar. Fourier transform infrared and extended X-ray absorption fine structure analysis at the Ti K edge reveals that the pillared titania exists in the form of anatase-structured TiO_2 nanocrystals, not in the form of covalently bonded mixed particles of TiO_2−SiO_2. On the basis of the present findings, we are able to conclude that the quantum-sized TiO_2 and SiO_2 particles are independently intercalated to form a multilayer stacking intracrystalline structure in the gallery space of aluminosilicate clay.

Introduction

Smectite-type clay minerals are composed of regularly stacked two-dimensional aluminosilicate layers with reactive interlayer spaces, giving rise to various intercalation compounds by an ion exchange reaction. In particular, the aluminosilicate layers pillared with inorganic polyoxyhydroxy cations such as $[Al_{13}O_4(OH)_{24}]^{7+}$, $[Zr_4(OH)_{14}]^{2+}$, $[Cr_n(OH)_m]^{3n-m}$, $[Bi_6(OH)_{12}]^{6+}$, $[Fe_3O(OCOCH_3)_6]^{+}$, and $[Ga_{13}O_4(OH)_{24}]^{7+}$ are of great interest due to their high catalytic activity.[1−5] Such pillared compounds, therefore, have been considered as useful catalysts, catalyst−supports, molecular sieves, selective adsorbents, membranes, and sensor materials.[6−10] Recently mixed sol particles such as SiO_2−TiO_2, SiO_2−Fe_2O_3, and SiO_2−ZrO_2 have been used as pillaring species, leading to the enhancement of thermal stability of the resulting pillared clays. Also, the sol particle pillared clays could have a very large Brunauer−Emmett−Teller (BET) specific surface area of 500−900 m^2/g and excellent thermal stability up to 800 °C.[11−13] In particular, the SiO_2−TiO_2 pillared clay has attracted special interest due to its photocatalytic activity on the oxidative photodegradation of various environmental pollutants such as halogenated hydrocarbons, pesticides, surfactants, etc.[14−16] From the viewpoint of photocatalysis, it is very important not only to characterize the porous structure of pillared clays but also to understand the bonding character and the electronic structure of TiO_2 pillar. However, there has been no systematic study on the chemical bonding nature of pillared TiO_2 nanoparticles in the SiO_2−TiO_2 pillared clay.

In this study, we have prepared highly porous pillared clay compounds with multilayered SiO_2−TiO_2 nanosol particles and characterized their electronic and crystal structures and porosity in detail. In particular, special attention has been paid in determining the intracrystalline pillar structure of porous nanohybrid in order to elucidate the pillaring mechanism using various spectroscopic methods such as Fourier transform infrared (FT-IR), UV−vis, and X-ray absorption fine structure (XAFS) techniques.

Experimental Section

Preparation of Porous Nanohybrid. Na^+-activated montmorillonite (Vol clay; American Colloidal Co.) with a layer charge of 0.29 $e^-/(Si, Al)_4O_{10}$ was used as a two-dimensional host. The 1.0 wt % aqueous suspension of montmorillonite was preswelled for 1 day before the ion-exchange reaction. A silica sol solution was prepared by mixing $Si(OC_2H_5)_4$, 2 N HCl, and ethanol in the volume ratio of 13.6/3.5/3.0 at room temperature. Also, titanium isopropoxide, $Ti(OC_3H_7)_4$, was hydrolyzed by adding into 1 N HCl solution with a molar ratio of HCl/Ti-$(OC_3H_7)_4$ = 6. The resulting translucent slurry was aged to obtain a clear sol solution by continuous stirring for 30 min at room temperature. Then the prepared silica and titania sol solutions were mixed with a molar ratio of Si/Ti = 10/1, stirred further for 1 h at room temperature, and finally titrated into the colloidal suspension of montmorillonite with a ratio of Si/Ti/montmorillonite = 20 mmol/2 mmol/1 g. The mixture was then allowed to stand for 30 h at 65 °C to exchange Na^+ ions in the montmorillonite with the positively charged SiO_2 and TiO_2 sol particles. The reaction product was separated by centrifugation, washed thoroughly with deionized water (hereafter abbreviated as STPC-wet), and then dried in an oven at 80 °C for 24 h (hereafter abbreviated as STPC-80). To complete the pillaring reaction, the sample of STPC-80 was calcined at 300, 400, and

* To whom correspondence should be addressed. E-mail: jhchoy@ewha.ac.kr. Tel: +82-2-3277-4135. Fax: +82-2-3277-4340.
† Seoul National University.
‡ Ewha Womans University.

10.1021/jp055601x CCC: $33.50
Published on Web 01/10/2006

TABLE 1: pH, Temperature, and the Surface Charge of Particle in the Precursor Solutions and Reaction Media for the Synthesis of SiO_2-TiO_2 Pillared Clay

	TiO_2 sol solution	SiO_2 sol solution	mixed sol solution	Na^+−montmorillonite suspension[a]	reaction solution (1)[b]	reaction solution. (2)[c]
pH	0.1	0.3	0.2	8.1	1.0	0.9
temp (°C)	20	20	20	20	20	60
surface charge	+	+	+	−		

[a] 1 wt % montmorillonite suspension. [b,c] Ion exchange reactions in the mixed solution consisted of Na^+−montmorillonite suspension and SiO_2-TiO_2 sol at 20 and 65 °C, respectively.

500 °C for 2 h (hereafter abbreviated as STPC-300, STPC-400, and STPC-500, respectively).

Sample Characterization. Powder X-ray diffraction (XRD) patterns for the samples deposited on a slide glass were taken using a Philips PW1830 diffractometer with Ni-filtered Cu Kα radiation ($\lambda = 1.5406$ Å) operated at 40 kV and 20 mA. Chemical analyses for the starting clay and its pillared samples were carried out by the inductively coupled plasma (ICP, Shimadzu ICPS-5000) method. For the chemical analysis, the aqueous solution of the aluminosilicates was prepared by dissolving the fused product of the clay sample and lithium metaborate in a 3% HNO_3 solution. FT-IR spectra were recorded in the range 400−1600 cm^{-1} from the mixture pellet of the clay sample and KBr with a FT-IR spectrophotometer Bomem Michelson MB-102-C15. Diffuse reflectance UV−vis spectra were recorded on a Perkin-Elmer Lambda 12 spectrophotometer equipped with an integrating sphere of 60 mm in diameter using $BaSO_4$ as a standard. To analyze porous properties, nitrogen adsorption−desorption isotherms were measured volumetrically at liquid nitrogen temperature by a homemade computer-controlled measurement system.[11] The adsorption−desorption isotherms of solvents such as water, methanol, and toluene were also measured gravimetrically at 25 °C using a CAHN-1000 balance. All the samples were degassed at 300 °C for 2 h under vacuum prior to the sorption measurements.

XAFS experiments were carried out at the Ti K-edge with the extended X-ray absorption fine structure (EXAFS) facility installed at beam line 7C at the Photon Factory, High Energy Accelerator Research Organization (KEK, Tsukuba), operated at 2.5 GeV with 300−400 mA electron current.[17] All the data were recorded in a transmission mode at room temperature using a Si(*111*) double-crystal monochromator with focusing mirrors. The intensities of incident and transmitted beams were measured with N_2 and Ar (25%) + N_2 (75%) filled ionization chambers, respectively. To ensure the spectral reliability, much care was made to evaluate the stability of energy scale by monitoring the spectrum of Ti metal for each measurement. The edge position was found to be reproducible to better than 0.05 eV. The data analyses for experimental spectra were performed by the standard procedure as follows:[18,19] Inherent background in the data was removed by fitting a polynomial to a pre-edge region and then extrapolating it through an entire spectrum and finally subtracting this fitted background from the entire spectrum. The resulting spectra, μ(E), were normalized to an edge jump of unity for comparing X-ray absorption near edge structure (XANES) features directly with one another. The absorption spectrum for an isolated atom, $\mu_0(E)$, was approximated by a cubic spline function. The EXAFS function, $\chi(E)$, was then expressed as $\chi(E) = \{\mu(E) - \mu_0(E)\}/\mu_0(E)$. Further analysis was performed in both k and R spaces, and the photoelectron wave vector was defined as $k = \{(8\pi^2 m_e/h^2)(E - E_0)\}^{1/2}$, where m_e is the electron mass and E_0 is the threshold energy determined as 4980 eV at half-height of the absorption edge jump. The resulting EXAFS spectra were k^3 weighted to compensate for the attenuation of the EXAFS amplitude at high k and then Fourier transformed in the range $\sim 1.0 \le k \le \sim 12$ $Å^{-1}$ with a Hanning apodization function of $dk = 0.5$ $Å^{-1}$. To determine structural parameters, nonlinear least-squares curve fitting was performed in the range $R \le 4$ Å using the UWXAFS code.[20,21] The backscattering amplitude, the phase shift, and the photoelectron mean free path were theoretically calculated for all scattering paths including multiple scattering paths by the curved wave ab initio EXAFS code FEFF6.[22,23] In the course of nonlinear least-squares curve fitting between experimental and theoretical spectra, the structural parameters such as bond distance, Debye−Waller factor, coordination number (CN), and threshold energy difference were set as variables. To quantitatively determine the effect of intercalation on the CN of Ti atoms, the amplitude reduction factors obtained from anatase TiO_2 reference were used for the CN estimation of the pillared compounds.

Results and Discussion

SiO_2-TiO_2 Mixed Oxide Nanosol Particles. Silica sol particles could be intercalated into aluminosilicate layers by the deposition of positively charged titania sols on their surface, leading to the modification of surface charge from negative to positive.[12] Although the surface charge of silica sol particle has been known to be negative in a broad pH domain (pH > 2), it becomes positive under a strong acidic condition (pH < 1).[24−27] In terms of a significant correlation between pH and surface charge, it is necessary to monitor the proton concentration during intercalation reaction. Thus, the solution pH was carefully measured at the various stages of intercalation reaction to characterize the surface potential of colloidal particles in a sol solution. As summarized in Table 1, the pH values of SiO_2 and TiO_2 sol solutions and the mixture of both solutions are all less than 1. Since the isoelectric points of SiO_2 and TiO_2 sol particles are at around 2.5 and 6, respectively,[24,25] the surface charges of particles in both sol solutions would be positive. By consideration of the fact that the surface potential of TiO_2 particles is more positive than that of SiO_2 particles, we could propose an intercalation mechanism, in which TiO_2 sol particles are more preferentially incorporated into negatively charged aluminosilicate than SiO_2 particles.

Layered Nanohybrid with SiO_2-TiO_2 Sol Particles. Powder XRD analysis reveals that the basal spacing of layered aluminosilicate increases greatly to a value of approximately 51 Å upon intercalation of sol particles, as shown in Figure 1. Since the gallery height (41 Å) is substantially larger than the basal spacing of clay itself (~9.6 Å), the STPC can be regarded as a "supragallery" pillared clay. The expanded basal spacing upon intercalation is maintained after a heat treatment at 500 °C, underscoring the excellent thermal stability of the obtained pillared clay. The atomic compositions of Na^+−montmorillonite and PILCs have been quantitatively analyzed by ICP. With an assumption that the chemical composition of montmorillonite remains unchanged before and after the pillaring reaction, the pillar composition of PILCs could be estimated to be $(TiO_2)_{0.82}$-

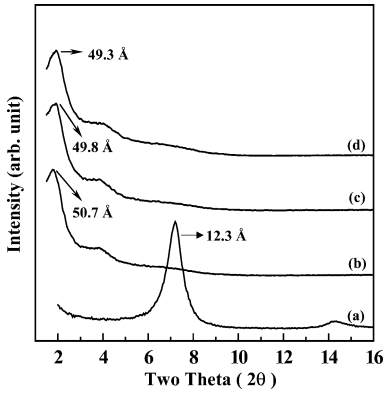

Figure 1. Powder XRD patterns for (a) pristine Na^+−montmorillonite, (b) STPC-300, (c) STPC-400, and (d) STPC-500, respectively.

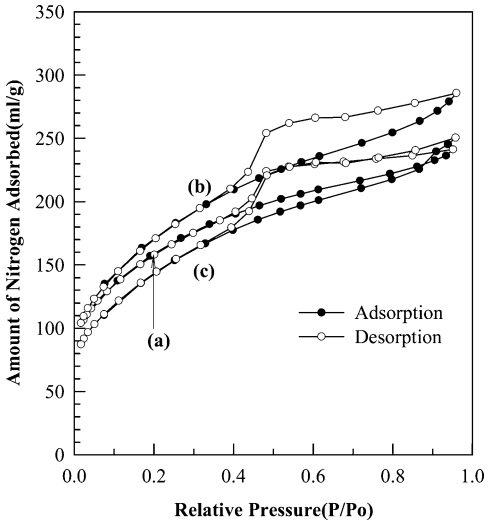

Figure 2. Nitrogen adsorption−desorption isotherms for (a) STPC-300, (b) STPC-400, and (c) STPC-500.

$(SiO_2)_{5.31}$ on the $O_{10}(OH)_2$ unit basis of aluminosilicate layers. Also, the Ti/Si molar ratio (∼0.15) of intercalated sols appears to be higher than the nominal value (∼0.10) in the precursor solution of mixed sol particles, indicating that the TiO_2 sol particles exhibit a stronger affinity for the negatively charged aluminosilicate layers than the SiO_2 particles. This finding is in good agreement with our expectation based on the isoelectric points of SiO_2 and TiO_2 sols.

Gas and Solvent Adsorption−Desorption Isotherms. Figure 2 shows the nitrogen adsorption−desorption isotherms of STPCs calcined at various temperatures. All the isotherms can be characterized as the mixed type between type I and IV according to the BDDT (Brunauer, Deming, Deming, and Teller) classification with a large hysteresis, whose features correspond to the type B in Boer's five types representing the presence of open slit-shaped pores.[28,29] In particular, STPC-400 shows the largest nitrogen adsorption capacity of 0.46 mL/g with a specific BET surface area of 590 m^2/g. To evaluate the microporosity of STPCs, *t*-plot analysis was carried out using the adsorption branch, as plotted in Figure 3a. In the present plots, the content of adsorbed nitrogen is presented as a function of statistical thickness, *t*, obtained from a standard *t*-curve of Harkins−Jura equation.[29] The micropore volume (V_{micro}) is estimated using the line extrapolated from the high-pressure branch to the adsorption axis, and the slit width is determined by doubling the *t*-value of the inflection point, which deviates downward from the high-pressure branch. The slit widths are estimated to be about 12 Å for all the STPCs (Table 2). The inflection points

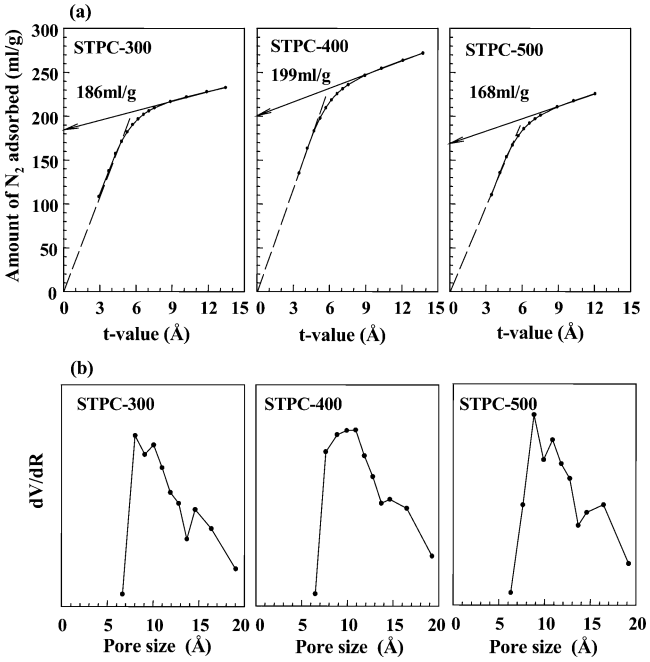

Figure 3. (a) *t* plots and (b) MP diagrams calculated from nitrogen adsorption isotherms for STPC-300, STPC-400, and STPC-500.

TABLE 2: Porosity Parameters for the Pristine Na^+−Montmorillonite and SiO_2−TiO_2 Pillared Clays Calcined at 300−500 °C

sample	specific surface area S_{BET} (m^2/g)	slit width (Å)	V_t (ml/g)[a]	V_{micro} (ml/g)[b]
Na^+−Montmorillonite	30		0.05	
STPC-300	525	11.8	0.38	0.28
STPC-400	590	12.2	0.46	0.31
STPC-500	504	12.0	0.41	0.26

[a] V_t = total pore volume. [b] V_{micro} = micropore volume.

in the *t* plots show a smooth variation in the range of 4.0−8.0 Å, corresponding to a slit width of 8.0−16.0 Å. This observation is in good agreement with the results of micropore analysis (MP)[29] revealing the pore size of 8.0−16.0 Å (Figure 3b).

To probe the chemical nature of the internal surface of pores in STPC, the sorption isotherms for water, methanol, and toluene were recorded at room temperature. As shown in Figure 4, the adsorption−desorption behavior of water is very similar to that of methanol; the adsorption rates for both solvents increase linearly with the relative vapor pressure. Since the desorption branches do not meet the adsorption branch even at a very low relative pressure, irreversible chemical reactions such as grafting of alcohol, hydroxylation, and/or hydration seem to occur during adsorption. Both the adsorption isotherms can be well reproduced with the BET equation rather than with the Langmuir one, indicating that a large number of pores can be filled by the multilayer adsorption of methanol or water molecules. On the contrary, the adsorption isotherm for toluene shows a typical BDDT type-I shape, which can be well reproduced by the Langmuir linear equation than the BET one. In this regard, the multilayer adsorption of toluene is physically difficult in the internal surface of pores. By consideration of the relatively larger molecular size of toluene (the van der Waals diameter = 6.8 Å), the pore sizes of STPCs should be in the range 6.8−13.6 Å, which is in good agreement with the slit width (12 Å) estimated from the *t*-plot analysis. A steep adsorption of toluene appears at low relative pressure, which is ascribed to a pore filling by toluene through a strong interaction between nonpolar

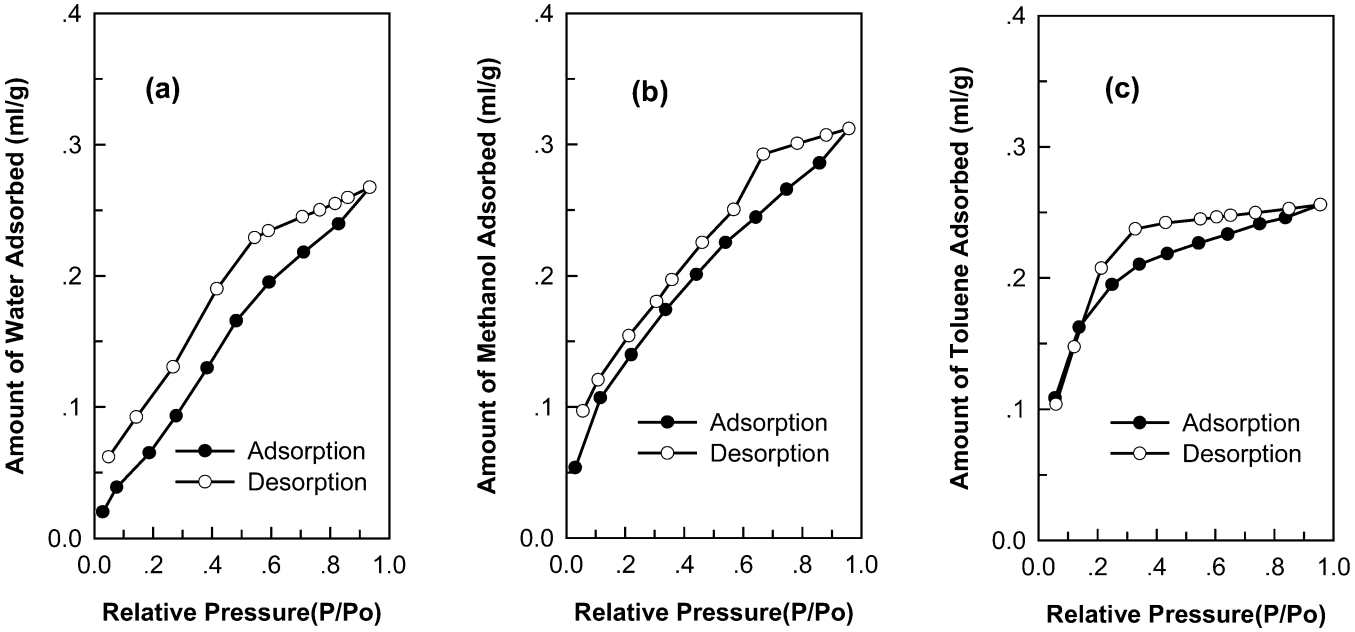

Figure 4. Various solvent adsorption−desorption isotherms for STPC-400: (a) water, (b) methanol, and (c) toluene.

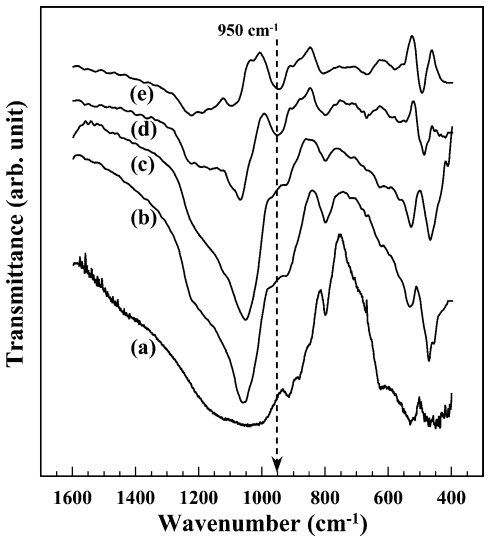

Figure 5. FT-IR transmittance spectra for (a) Na^+−montmorillonite, (b) STPC-80, (c) STPC-300, (d) STPC-400, and (e) STPC-500.

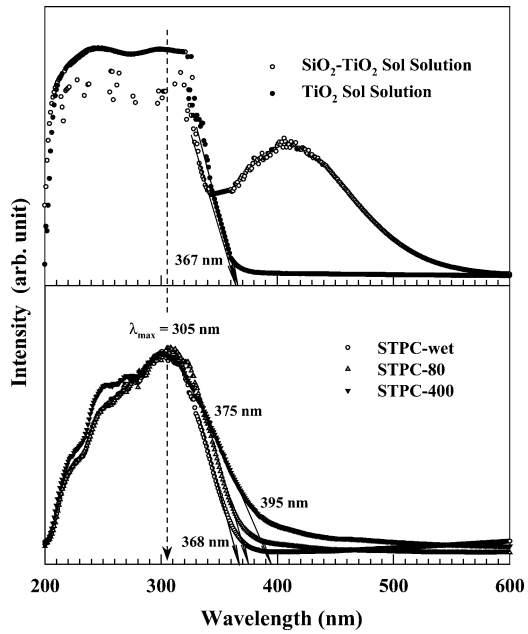

Figure 6. UV−vis spectra for TiO_2 sol and SiO_2-TiO_2 sol solution and STPC-wet, STPC-80, and STPC-400.

toluene molecules and the hydrophobic pore surface. The hydrophobic nature of the internal pore surface is mainly due to the loss of layer charge of montmorillonite upon pillaring reaction.

FT-IR and UV−Vis Spectroscopy. To understand the pillaring mechanism of nanosized SiO_2 and TiO_2 sol particles in the interlayer space of montmorillonite, FT-IR spectra were measured for the pristine Na^+−montmorillonite and its pillared compounds calcined at various temperatures, as shown in Figure 5. The absorption band at ca. 950 cm^{-1} corresponding to the vibration of (Si−O−Ti) bond is absent in the spectrum of the STPC-80, but it appears after calcinations at higher than 400 °C.[30] This finding provides strong evidence that the TiO_2 sol particles are independently intercalated without any distinct chemical bonding with the co-intercalated SiO_2 sol particles. It is necessary to heat the sample up to 400 °C to form the covalent (Si−O−Ti) bond between titania and layered silicate or between titania and silica.

We have carried out UV−vis spectroscopic analysis not only to examine the electronic structure of the pillared compounds but also to estimate the particle size from a shift of absorption edge. The UV−vis spectra of STPC-wet, STPC-80, and STPC-400 are represented in Figure 6, together with those of TiO_2 sol solution and mixed SiO_2-TiO_2 sol solution. All the present samples exhibit a prominent blue shift of absorption edge compared to bulk rutile and anatase TiO_2, which is surely due to the formation of quantum-sized TiO_2.[31−33] The optical absorption could be characterized by two different energies, namely, λ_{max} corresponding to the position with maximum absorption and an absorption threshold energy corresponding to the position of a steep increase of absorption. The λ_{max} and the absorption threshold energy of TiO_2 sol solution are determined to be 305 and 367 nm, respectively. From the relationship between these values and particle size, we could estimate the particle size of TiO_2 as 20 Å.[32,33] Similar values of the λ_{max} and the absorption threshold were obtained for the SiO_2-TiO_2 mixed sol solution and STPC-wet, indicating

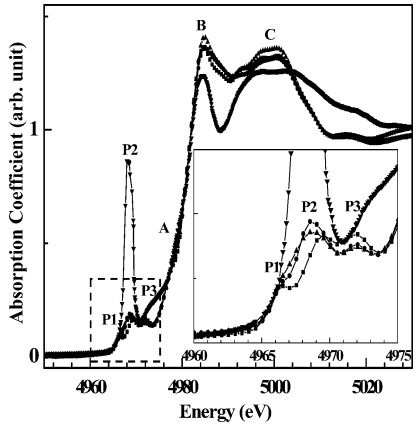

Figure 7. Normalized Ti K-edge XANES spectra for STPC-80 (circles), STPC-400 (triangles), anatase TiO_2 (squares), and $BaTiO_4$ (inverse triangles).

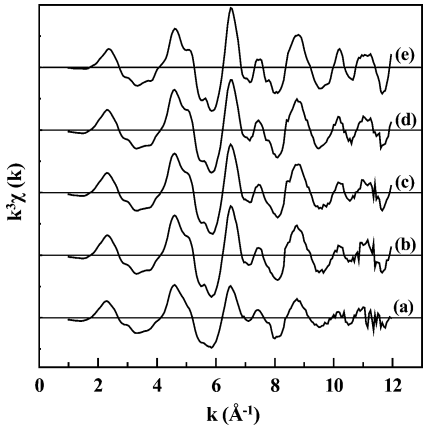

Figure 8. Experimental k^3-weighted Ti K-edge EXAFS spectra for (a) STPC-80, (b) STPC-300, (c) STPC-400, (d) STPC-500, and (e) anatase TiO_2.

negligible change of TiO_2 particle size upon the mixing with SiO_2 sol solution and intercalation into clay lattice. After drying and subsequent calcination of the STPC-wet, a distinct red shift of absorption edge occurs due to the coagulation of the intercalated TiO_2 sol particles and/or to a formation of Si−O−Ti ionocovalent bonds among titania, silica, and aluminosilicate lattice.

Ti K-Edge XANES/EXAFS Analysis. Figure 7 shows the Ti K-edge XANES spectra for STPC-80 and STPC-400, together with the reference spectra of anatase TiO_2 and Ba_2TiO_4. The overall spectral shapes of the pillared STPC compounds are very similar to those of the anatase TiO_2, suggesting the structural similarity among these compounds. While the pre-edge peaks P_1, P_2, and P_3 related to the dipole-forbidden 1s → 3d transitions are fairly weak in intensity for the pillared compounds and the reference TiO_2, a very intense feature P_2 is detected for the reference Ba_2TiO_4 with a tetrahedral TiO_4 unit. Judging from the fact that this peak gains a significant spectral weight in case of noncentrosymmetric geometry through a mixing of 3d and 4p orbitals,[34,35] the relatively weak intensity of these features suggests the pseudo-octahedral symmetry of titanium in the pillared compounds. A close inspection on the pre-edge region reveals that the pillared compounds show more intense peak P_2 corresponding to the 1s → t_{2g} transition than the bulk anatase TiO_2 with a red shift of ∼0.8 eV. It was well documented that the intensity and energy of the peak P_2 can provide an indicator for differentiating four-, five-, and six-coordinated titanium ions.[36] With a reference to a previously reported diagram between the peak position and intensity,[36] the present STPC-400 compound was found to have 20% of the five coordinated titanium ions and 80% of the six coordinated ones. This finding provides strong evidence on the presence of coordinatively unsaturated Ti sites due to the nanocrystalline nature of the titania in the pillared compound.[37] In addition to the pre-edge peaks, there are several main-edge and post-edge features (denoted A, B, and C) corresponding to the dipole-allowed 1s → 4p transitions. Among them, the peak B can be interpreted as the transition to unoccupied 4p orbitals, whereas the other main-edge feature A at lower energy would originate from the transition with shakedown process.[34,35] As in the pre-edge region, the pillared compounds show similar spectral shape in the main-edge region to the anatase TiO_2.

Figure 8 represents the Ti K-edge k^3-weighted EXAFS spectra for STPC-80, STPC-300, STPC-400, STPC-500, and anatase TiO_2 and the corresponding Fourier transforms (FTs) are plotted in Figure 9. The overall spectral features in the raw data and

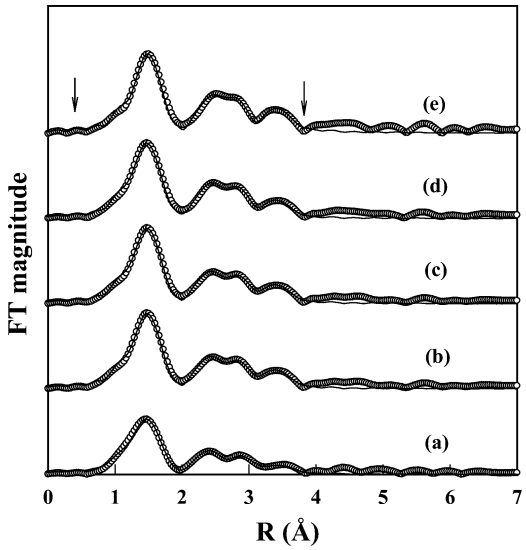

Figure 9. Fourier transforms of EXAFS spectra for (a) STPC-80, (b) STPC-300, (c) STPC-400, (d) STPC-500, and (e) anatase TiO_2. Their best-fitted spectra (solid lines) are compared with experimental spectra (open circles). The Fourier filtering range is shown by the arrows.

FT spectra of the STPCs are nearly identical to those of the anatase TiO_2, highlighting structural similarity among the present compounds. While the first FT peak at ∼1.5 Å originates from the closest (Ti−O) coordination shell, the more distant features at ∼2.5 and ∼3.5 Å are related to (Ti−Ti) bonding pairs in edge- or corner-shared TiO_6 octahedra, respectively. To determine detailed structural parameters, a nonlinear least-squares curve fitting was performed for these three FT peaks in the range $R \leq 4$ Å. With a reference to the crystal structure of the anatase TiO_2 phase, four single scattering paths of Ti−O(1), Ti−Ti_{edge}, Ti−Ti_{corner}, and Ti−O(2) were used to reproduce the experimental EXAFS data. As shown in Figures 9 and 10, all the experimental spectra of the pillared compounds are well reproduced with anatase TiO_2 structure, clearly demonstrating that the pillared titania exists in the form of the anatase nanoparticle, not in the form of covalently bonded particle of TiO_2−SiO_2. No FT peak corresponding to the Si−O−Ti bond appears in the data of STPC-400 and STPC-500, which seems not to be compatible with the FT-IR results. Such a discrepancy would be due to the fact that the Si−O−Ti bond is partially formed on the surface of TiO_2 nanoparticles not in the bulk, and hence it is not detectable by the EXAFS analysis reflecting the bulk state. The obtained structural parameters are sum-

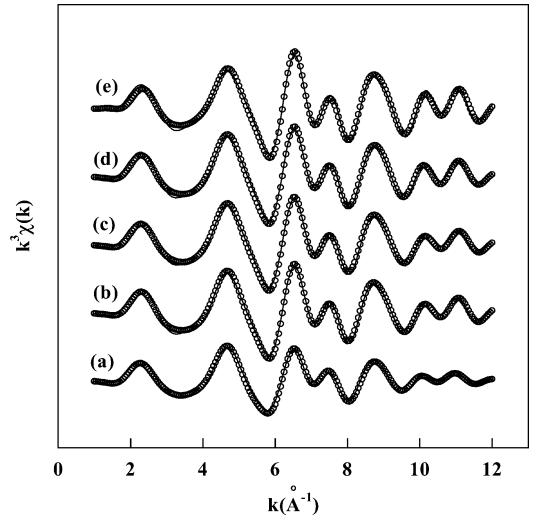

Figure 10. Experimental Fourier-filtered $k^3\chi(k)$ spectra (open circles) and their best fits (solid lines) for (a) STPC-80, (b) STPC-300, (c) STPC-400, (d) STPC-500, and (e) anatase TiO_2.

TABLE 3: Ti K-edge EXAFS Fitting Results for SiO_2-TiO_2 Pillared Clays Calcined at 80−500 °C and the Reference Anatase TiO_2

sample	atom pairs	CN[a]	R[b]	DW[c]	ΔE_0[d]
STPC-80	Ti−O(1)	5.7	1.95	8.92	−0.87
	Ti−Ti(1)	3.1	3.02	7.50	−2.00
	Ti−Ti(2)	2.8	3.78	4.58	−0.64
	Ti−O(2)	7.2	3.89	1.83	−1.75
STPC-300	Ti−O(1)	6.4	1.95	6.78	−0.78
	Ti−Ti(1)	3.8	3.02	6.11	−0.31
	Ti−Ti(2)	3.4	3.78	5.94	−2.92
	Ti−O(2)	7.4	3.87	1.64	−1.91
STPC-400	Ti−O(1)	6.4	1.95	7.05	−0.79
	Ti−Ti(1)	3.8	3.01	6.24	−0.90
	Ti−Ti(2)	3.3	3.77	5.46	−3.33
	Ti−O(2)	7.4	3.87	1.58	−2.43
STPC-500	Ti−O(1)	6.7	1.95	7.21	−0.81
	Ti−Ti(1)	3.8	3.02	5.30	−0.40
	Ti−Ti(2)	3.4	3.78	5.70	−3.66
	Ti−O(2)	7.6	3.87	1.42	−1.98
anatase TiO_2	Ti−O(1)	6.0	1.95	5.55	−0.36
	Ti−Ti(1)	4.0	3.02	5.19	1.56
	Ti−Ti(2)	4.0	3.79	7.64	0.70
	Ti−O(2)	8.0	3.86	1.59	−2.60

[a] Coordination numbers estimated with amplitude reduction factor from the reference anatase TiO_2. [b] Interatomic distance (R, Å). [c] Debye−Waller factor (σ^2, 10^{-3} Å^2). [d] Energy shift (ΔE_0, eV).

marized in Table 3. While the bond distances of the pillared compounds were determined to be almost the same as those of the anatase TiO_2, the CNs of the edge- and corner-shared (Ti−Ti) shells are smaller for the formers than for the latter, as suggested from the XANES results. From the present XANES/EXAFS results, the pillared titania species are stabilized as quantum-sized TiO_2 nanoparticles with an anatase structure, which is in a good agreement with the blue shift of band-gap energy.

Conclusion

Highly porous nanohybrids have been successfully prepared by an ion exchange reaction of the Na^+ ions in montmorillonite with the positively charged SiO_2 and TiO_2 sol particles. The adsorption−desorption isotherms of nitrogen and various solvent vapors showed the STPC calcined at 400 °C to have a large BET surface area up to 590 m^2/g and a porosity of 0.46 mL/g. Most of the porosity of the STPC originates from micropores of ca. 12 Å with a hydrophobic surface property. According to UV−vis, FT-IR, and XAFS analyses, the intercalated titania species exist as anatase-type TiO_2 nanoparticles without linking with the co-intercalated SiO_2 particles. A thermal treatment beyond 400 °C is found to be necessary to complete the pillaring reaction through the formation of the Si−O−Ti bond. The stabilization of quantum-sized TiO_2 nanoparticles in the two-dimensional lattice of aluminosilicate makes the present porous compound a promising candidate for efficient photoctalysts and electrodes for high efficiency solar cells.

Acknowledgment. This work was financially supported by Korean Research Foundation Grant (KRF-2004-041-C00187) and in part by the SRC/ERC program of MOST/KOSEF (Grant R11-2005-008-01001-0). We thank Prof. M. Nomura of the Photon Factory for his help in performing the synchrotron radiation experiments.

References and Notes

(1) (a) Pinnavaia, T. J.; Landau, S. D.; Tzou, M. S.; Johnson, I. D. *J. Am. Chem. Soc.* **1985**, *107*, 7222. (b) Jones, S. L. *Catal. Today* **1987**, *12*, 209.

(2) (a) Pichowicz, M.; Mokaya, R. *Chem. Mater.* **2004**, *16*, 263. (b) Hernando, M. J.; Pesquera, C.; Gonzaléz, F. *Langmuir* **2001**, *17*, 5156.

(3) Volzone, C.; Cesio, A. M.; Sanchez, R. M. T.; Peria, E. *Clays Clay Miner.* **1993**, 41, 702.

(4) Kloprogge, J. T.; Booy, E.; Jansen, J. B. H.; Geus, J. W. *Clay Miner.* **1994**, *29*, 153.

(5) (a) Yamanaka, S.; Doi, T.; Sako, S.; Hattori, M. *Mater. Res. Bull.* **1984**, *19*, 161. (b) Ohtsuka, K. *Chem. Mater.* **1997**, *9*, 2030. (c) Lee, S. R.; Park, M.; Han, Y. S.; Hwang, S. H.; Choy, J. H. *J. Phys. Chem.* B **2005**, *109*, 9432.

(6) Suib, S. L.; Occelli, M. L.; Tanguay, J. F. *J. Am. Chem. Soc.* **1986**, *108*, 6972.

(7) Giannelis, E. P.; Pinnavaia, T. J.; Rightor, E. G.*J. Am. Chem. Soc.* **1988**, *110*, 3880.

(8) Rudzinski, W. E.; Bard, A. J. *J. Electroanal. Chem.* **1986**, *199*, 323.

(9) Dobil, C.; Mathews, J. F.; Turney, T. W. *Catal. Lett.* **1994**, *23*, 151.

(10) (a) Pires, J.; Pinto, M. L.; Carvalho, A.; de Carvalho, M. B. *Langmuir* **2003**, *19*, 7941. (b) Bourlinos, A. B.; Karakassides, M. A.; Simopoulos, A.; Petridis, D. *Chem. Mater.* **2000**, *12*, 2640. (c) Yoneyama, H.; Hago, S.; Yamanaka, S. *J. Phys. Chem.* **1989**, *12*, 4833.

(11) Choy, J.-H.; Park, J.-H.; Yoon, J.-B. *J. Phys. Chem. B* **1998**, *31*, 5991.

(12) Yamanaka, S.; Inoue, Y.: Hattori, M.; Okumura, F.; Yoshiikawa, M. *Bull. Chem. Soc. Jpn.* **1992**, *65*, 2494.

(13) Takahama, K.; Yokoyama, M.; Hirao, S.; Yamanaka, S.; Hattori, M. *J. Mater. Sci.* **1992**, *27*, 1297.

(14) Grätzel. CK.; Grätzel. M.; Jirousek. M.; *J. Mol. Catal.* **1987**, *39*, 347.

(15) Cuendet. P.; Grätzel. M. *J. Phy. Chem.* **1987**, *91*, 3550.

(16) Laurence, A.; Chantal, G.; Pierre, P. *J. Photochem. Photobiol. A: Chem.* **1995**, *85*, 257.

(17) Nomura, M.; Akoyana; Sakurai, M. *KEK Report* 9H099D.

(18) Teo, B. K. *EXAFS: Basic Principles and Data Analysis*; Springer-Verlag: Berlin, 1986.

(19) Sayers, D. E.; Bunker, B. A. In *X-ray Absorption: Principles, Applications, Techniques of EXAFS, SEXAFS, and XANES*; Koningsberger, D. C.; Prins, R., Eds.; Wiley-Intersciences: New York, 1988; pp 211−253.

(20) Newville, M.; Livins, P.; Yacoby, Y.; Rehr, J. J.; Stern, E. A. *Phys. Rev. B* **1993**, 47, 14126.

(21) Frenkel, A.; Stern, E. A.; Vornel, A.; Qian, M.; Newville, M. *Phys. Rev. B* **1994**, *45*, 11662.

(22) Rehr, J. J.; Mustre de Leon, J.; Zabinsky, S. L.; Albers, R. C. *J. Am. Chem. Soc.* **1991**, *113*, 5135.

(23) O'Day, P. A.; Rehr, J. J.; Zabinsky, S. L.; Brown, G. E., Jr. *J. Am. Chem. Soc.* **1994**, *116*, 2938.

(24) Brinker, C. J.; Scherer, G. W. *Sol−Gel Science: The Physics and Chemistry of Sol−Gel Processing*; Academic Press: San Diego, 1990.

(25) Werner, S.; Morgan, J. J. *Aquatic Chemistry: An Introduction Emphasizing Chemical Equilibria in Natural Waters*; Wiley-Intersciences: New York, 1981.

(26) Moini, A.; Pinnavaia, T. J. *Solid State Ionics* **1988**, *26*, 119.
(27) Endo, T.; Moritland, M. M.; Pinnavaia, T. J. *Clays Clay Miner.* **1981**, *29*, 153.
(28) Gregg, S. J.; Sing, K. S. W. *Adsorption, surface Area and Porosity*; Academic Press: London, 1982.
(29) Allen, T. *Particle Size Measurement*, 4th ed.; Chapman and Hall: London, 1990.
(30) Lirong, Y.; Guoxing, Y. *J. Noncryst. Solid.* **1988**, *100*, 309.
(31) Anpo, M.; Shima, T.; Kodama, Kubokawa, S. Y. *J. Phys. Chem.* **1987**, *91*, 4305.
(32) Kormann, C.; Bahnemenn, D. W.; Michael, R.; Hoffmann, W. M. *J. Phys. Chem.* **1988**, *92*, 5196.
(33) Doherty, S.; Fitzmaurice, D. *J. Phys. Chem.* **1996**, *100*, 10732.
(34) Hur, S. G.; Park, D. H.; Kim, T. W.; Hwang, S. J. *Appl. Phys. Lett.* **2004**, *85*, 4130.
(35) (a) Ruiz-Lopez, M. F.; Munoz-Pzez, A. *J. Phys.: Condens. Matter.* **1991**, *3*, 8981. (b) Grunes, L. A. *Phys. Rev. B* **1983**, *27*, 2111.
(36) Farges, F.; Brown, G. E., Jr.; Rehr, J. J. *Phys. Rev. B* **1997**, *56*, 1809.
(37) Sanchez, M.; Garcia, C. J.; Mayoral, J. A.; Blasco, J.; Proietti, M. G.; *J. Mol. Catal.* **1994**, *92*, 311.